One-Dimensional Swelling of a pH-Dependent Nanostructure Based on ABC Triblock Terpolymers

Sabine Ludwigs,*,† Kristin Schmidt, and Georg Krausch

Physikalische Chemie II and Bayreuther Zentrum für Kolloide und Grenzflächen (BZKG), Universität Bayreuth, D-95440 Bayreuth, Germany

Received October 22, 2004; Revised Manuscript Received December 15, 2004

ABSTRACT: We present a novel route to prepare pH-dependent nanostructures from highly ordered thin films of poly(styrene)-*block*-poly(2-vinylpyridine)-*block*-poly(*tert*-butyl methacrylate) triblock terpolymers. Using a polymer-analogous reaction, we modify the chemical nature of the block components without altering the overall microdomain structure. In particular, we perform an acid-catalyzed hydrolysis of the poly(*tert*-butyl methacrylate) block to poly(methacrylic acid) in a microphase-separated perforated lamella (PL) structure. Scanning force microscopy in an aqueous environment is used to follow structural changes of the PL phase as a function of the pH value. Due to the particular microdomain structure of the precursor triblock terpolymer, an almost perfect one-dimensional swelling of the films is observed with increasing pH.

Introduction

In recent years the spontaneous formation of nanostructured materials by molecular self-assembly of block copolymers has received significant attention because of a wealth of potential applications. Block copolymers consist of two or more chemically different polymer blocks, which are covalently linked together to form a larger, more complex macromolecule. If the constituent polymers are immiscible, microphase separation is induced on a scale that is related to the size of the copolymer chains (i.e., in the range between 10 and 100 nm). Typical microdomain structures formed by diblock copolymers are cylinders, lamellae, and spheres. For triblock terpolymers the structural variety is much greater.[1] In the presence of boundary surfaces and confined to a thickness comparable to the characteristic bulk domain spacing, both large-scale alignment of the microdomain structures and stabilization of novel microdomain structures characteristic of thin films can be induced.[2−8] Only recently a variety of different novel thin film structures was found.[9]

The aligning effect of the interfaces, in particular, makes block copolymer thin film structures interesting for applications in nanotechnology.[10−15]

Well-defined patterning in thin films can also be used to prepare smart surfaces to serve as functional devices on the nanometer length scale. Some recent developments were aimed at strategies for the functionalization of surfaces with stimuli-responsive polymer brushes.[16] This approach is promising for applications in biosensors or nanofluidic devices, for example. Weak polyelectrolytes such as poly(methacrylic acid) undergo substantial changes in swelling in response to changes in pH or ionic strength, making them excellent candidates for smart surfaces that respond to specific stimuli.[16−20]

It is a challenging task to combine the rich variety of highly ordered nanostructures available in block copolymer thin films with the potential to create responsive structures by incorporation of suitable functional blocks. Synthesis of block copolymers containing stimuli-responsive blocks is well-established nowadays, and numerous groups have focused on the solution behavior of amphiphilic block copolymers, which contain at least one polyelectrolyte block.[21−28] Because of the large differences in solubility, however, amphiphilic block copolymer molecules tend to self-associate in aqueous solution and form micelles consisting of a hydrophobic core surrounded by a shell of the water-soluble blocks.[29−31] When cast from solution, such micellar structures often establish a significant kinetic barrier against the formation of what may be the desired melt equilibrium microdomain structure of the material. As a consequence, many of the complex microdomain structures typical for such materials both in the bulk and in thin films are not accessible via solvent casting of amphiphilic block copolymers.

This drawback can be overcome by self-assembly of a precursor block copolymer consisting of less incompatible blocks and subsequent chemical modification. Under suitable conditions, complex ordered microdomain structures can be formed in the precursor material and can be conserved during the following processing steps.[32] In the present paper we follow this pathway toward a pH-responsive block copolymer nanostructure. We start from a single layer of a highly ordered perforated lamella (PL) formed of a poly(styrene)-*block*-poly(2-vinylpyridine)-*block*-poly(*tert*-butyl methacrylate) triblock terpolymer.[33−36] After structure formation the poly(*tert*-butyl methacrylate) block is converted into poly(methacrylic acid) via a polymer-analogous hydrolysis reaction. Using scanning force microscopy in aqueous solutions, we map out lateral details of the morphology as a function of the pH value. We show that the overall *lateral* structure of the film is not affected by this reaction. However, above pH 6 the poly(methacrylic acid) chains are highly stretched and the film thickness increases to as much as 10 times the initial (dry) value. Due to the particular nature of the underlying PL structure the resulting polymer film expands in only a

* To whom correspondence should be addressed. E-mail: sabine.ludwigs@uni-bayreuth.de.

† Present address: Cavendish Laboratory, Department of Physics, University of Cambridge, Cambridge CB3 0HE, United Kingdom.

10.1021/ma047812q CCC: $30.25
Published on Web 02/22/2005

Scheme 1. Acid-Catalyzed Hydrolysis of PS-*b*-P2VP-*b*-PtBMA to PS-*b*-P2VP-H$^+$-*b*-PMAA

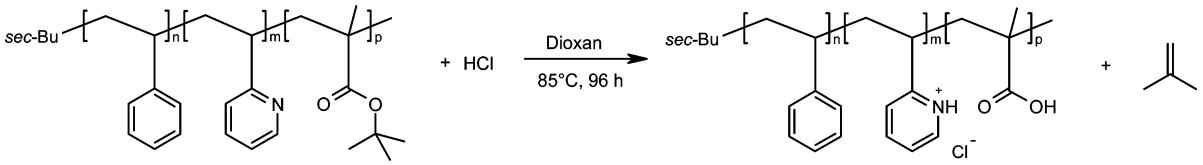

single dimension, making it a promising candidate as an actuator for potential nanotechnology applications.

Experimental Section

Thin Films of PS-*b*-P2VP-*b*-PtBMA Triblock Terpolymers. Various poly(styrene)-*block*-poly(2-vinylpyridine)-*block*-poly(*tert*-butyl methacrylate) triblock terpolymers were synthesized and characterized as reported previously.[33] Here we focus on a polymer which shows a core−shell cylindrical structure in the bulk. The overall molecular weight is M_w = 140 kg/mol, the polydispersity amounts to $M_w/M_n = 1.02$, and the volume fractions of the different blocks are $\phi_{PS} = 0.16$, $\phi_{P2VP} = 0.21$, and $\phi_{PtBMA} = 0.63$, respectively.

Thin films of this material were prepared on polished silicon wafers by spin coating from 5 mg/mL chloroform solutions. To further induce mobility, the samples were exposed to a well-controlled atmosphere of chloroform vapor for 20 h ($p_{CHCl_3} = 0.9p_0$, with p_0 being the vapor pressure of saturated chloroform at room temperature). During annealing, terraces of well-defined film thickness are formed which correspond to integer numbers of layers of energetically preferred microdomain structures. The resulting microdomain structures were quenched via fast solvent removal. Terraces with a film thickness of 37 ± 3 nm display a highly ordered perforated lamella structure. A systematic investigation of the thin film behavior of PS-*b*-P2VP-*b*-PtBMA triblock terpolymers has been recently performed.[34,35]

Acid-Catalyzed Hydrolysis of the PL Structure. Acid-catalyzed hydrolysis of PS-*b*-P2VP-*b*-PtBMA was accomplished by heating the films in the presence of a reservoir of 3 mL of HCl_{conc} for 12−15 h at a temperature of 60 °C. A similar approach has been recently performed for Langmuir−Blodgett films of PtBMA and poly(*tert*-butyl acrylate), aiming to produce PMAA and poly(acrylic acid), respectively.[37,38] Subsequently, the films were dried in a vacuum. The reaction yields the corresponding SVA triblock terpolymer with a poly(methacrylic acid) (PMAA) polyelectrolyte block. The driving force of this reaction is the elimination of gaseous isobutylene. Aside from the PtBMA hydrolysis, the reaction also yields the hydrochloride of the amine functionality of poly(2-vinylpyridine) (Scheme 1).

Characterization of Hydrolyzed Films. The degree of conversion of the hydrolysis reaction can be determined by FTIR spectroscopy. For a quantitative IR analysis the amount of material in the thin films was not sufficient. We therefore prepared homogeneous films with a thickness between 1 and 5 μm on silicon wafers by solvent casting. The films were subsequently hydrolyzed in the manner described above (without annealing in chloroform vapor). IR spectra of unhydrolyzed and hydrolyzed films have been directly taken on the silicon substrate, as silicon does not show IR absorption in the region of interest (1000−4000 cm^{-1}) (Figure 1).

Between 3500 and 2400 cm^{-1} the typical broad bands of the O−H vibration are obtained. The C=O absorption band at 1724 cm^{-1} is broadened and shifted to 1718 cm^{-1}. Hydrolysis also leads to a shift of C−O vibrations from 1254 and 1138 cm^{-1} to 1248 and 1162 cm^{-1}, respectively. Due to the acidic conditions during the preparation the pyridinium groups are protonated as can be seen by the N−H absorption band at 2560 cm^{-1} and the absorption bands of the aromatic vibrations, which are shifted from 1589 and 1568 cm^{-1} to 1616 and 1541 cm^{-1}, respectively. In addition, new bands appear at 994, 952, and 618 cm^{-1}. The disappearance of the *tert*-butyl double absorption band at 1394 and 1368 cm^{-1} is the most characteristic fingerprint of the reaction and can be used for a quantitative analysis.

In the micrometer thick specimens, the degree of hydrolysis has been determined to be approximately 91%. Since the films of interest for our study are less than 100 nm in thickness, it appears reasonable to assume complete hydrolysis under the same reaction conditions.

Scanning Force Microscopy in an Aqueous Environment. Thin films of PS-*b*-P2VP-H$^+$-*b*-PMAA on silicon wafers were investigated in the fluid cell of a MultiMode scanning force microscope (Digital Instruments, Veeco Group). We used contact-mode tips (Veeco NP-S cantilevers consisting of silicon nitride, spring constant k = 0.58 N/m). All experiments were performed in the TappingMode (resonance frequency $\omega \approx 10$ kHz). The water was filled into the liquid cell with a micropipet. For the pH-dependent measurements we exchanged the water in the cell with buffer systems. To avoid effects due to different counterions and ionic strengths,[39] we have chosen sodium phosphate buffers ($H_3PO_4/NaH_2PO_4/Na_2HPO_4/Na_3PO_4$) which allow pH variations in the range between pH 2 and pH 10. Prior to each measurement, the films were equilibrated for 30 min at a given pH value. For film thickness measurements scratches were applied to the polymer films after hydrolysis. Then the thickness of the film was determined relative to the substrate by scanning force microscopy.

Results and Discussion

Morphology of the Microstructure after Hydrolysis. Parts a and b of Figure 2 show SFM height images of a terpolymer film before and after acid-catalyzed hydrolysis. Before hydrolysis (Figure 2a), the film shows a rather flat surface with a hexagonal pattern of shallow dots, which are assigned to the perforated PL structure.[34,35] The film thickness in the dry state amounts to 37 ± 3 nm. The height difference between protrusions and valleys amounts to only 2 nm and most likely results from the drying conditions.[40] The inset to Figure 2a shows the sketch of a PL phase: Sheets of P2VP/PS/P2VP are perforated by channels of the majority component PtBMA which are connected between two outer layers of PtBMA, one of which is

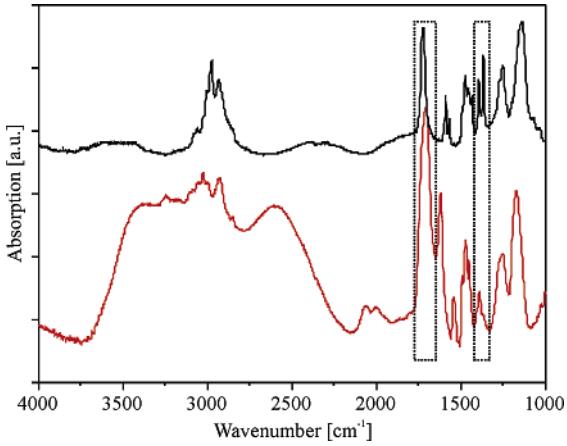

Figure 1. FTIR spectra before (black curve) and after (red curve) hydrolysis of a 3 μm thick film of PS-*b*-P2VP-*b*-PtBMA to PS-*b*-P2VP-H$^+$-*b*-PMAA.

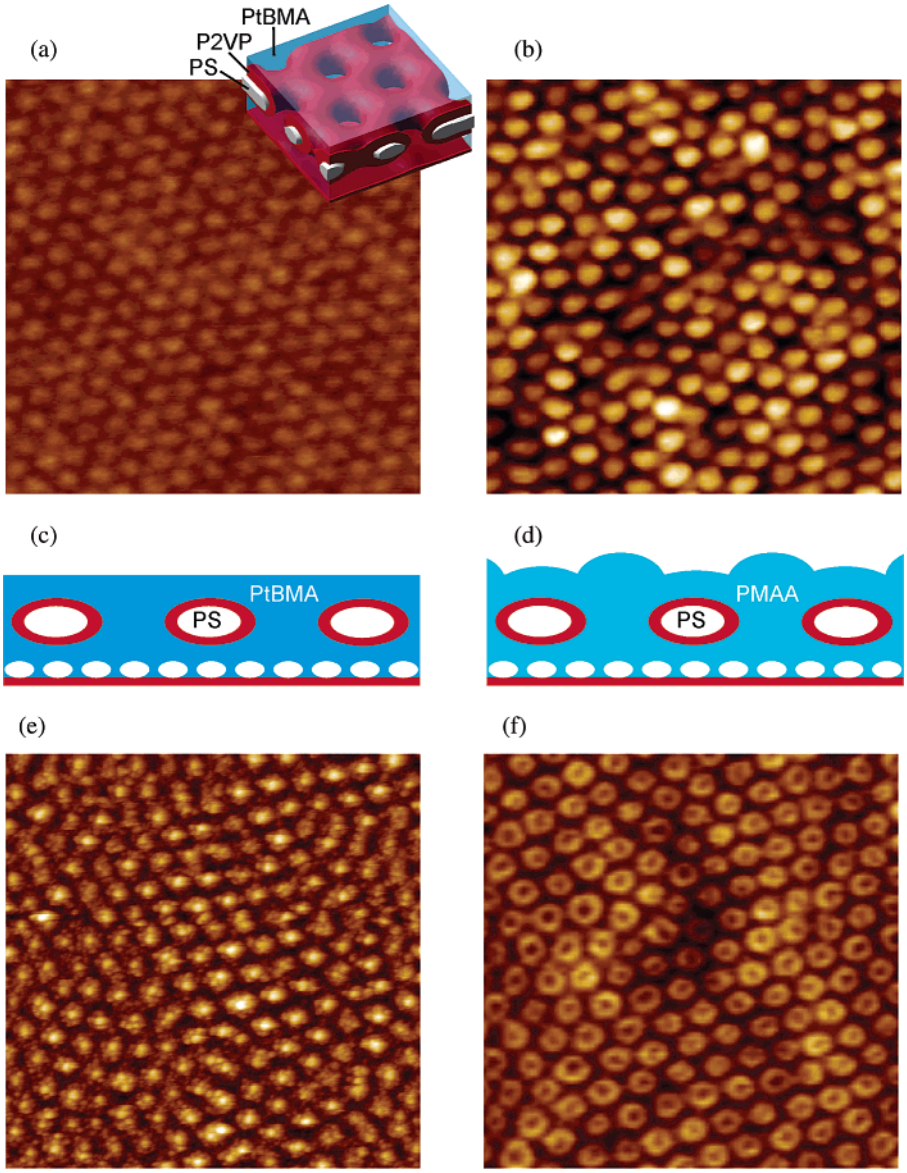

Figure 2. SFM height images of the PL structure before (a) and after (b) hydrolysis. The sketch in (a) corresponds to a MesoDyn simulation[34−36] of the first terrace of PL; the phases can be assigned to PS (white phase), P2VP (red phase), and PtBMA (blue phase). (c, d) Schematic cross-sections of a PL phase before and after hydrolysis. (e, f) SFM images of the PL structure after hydrolysis, taken in aqueous solutions (pH 6). The image size of the SFM images is $1 \times 1\ \mu m^2$. The height scale for (a) and (b) is $\Delta z = 0-10$ nm and for (e) and (f) $\Delta z = 0-30$ nm.

located at the air surface. Further details about the PL phase are provided in refs 34−36.

Figure 2b shows an SFM height image taken after hydrolysis at ambient conditions in air; the film thickness amounts to 26 ± 3 nm. For a detailed discussion of the film thickness see below. On first inspection, two major findings can be reported. Still a hexagonal arrangement of protrusions is clearly visible. Quantitative measurement of the characteristic spacing shows no significant difference from the virgin structure displayed in Figure 2a. However, the height of the protrusions has significantly increased to 12 nm. From these findings we conclude that the overall microdomain structure of the film is not affected by the HCl treatment. Since every block copolymer chain is locked by one end within a continuous (perforated) layer of polystyrene, which is not affected by the hydrolysis, major rearrangements of the block copolymer microstructure are not possible. However, during hydrolysis the P2VP block is protonated and the majority component PtBMA is modified to PMAA. Since PMAA is rather hygroscopic, the majority phase is expected to swell even at ambient conditions. Parts c and d of Figure 2 represent sketches of the microdomain structure before and after hydrolysis, respectively. Since the perforations of the PL phase contain more PtBMA (and, consequently, more PMAA after hydrolysis), the protrusions of the acid component are expected to form on top of the perforations of the P2VP/PS/P2VP lamella. Film thickness measurements reveal an overall shrinkage of the film thickness after acid saponification. Before hydrolysis the thickness of the first terrace of the PL phase amounts to $d_{SVT} = 37 \pm 3$ nm, while after hydrolysis the film thickness amounts to only $d_{SVA} = 26 \pm 3$ nm. As the films swell due to the water content in the air, the dry film

thickness of an SVA film should be even smaller. In the absence of water one would expect

$$d_{\mathrm{SVA}}^{\mathrm{dry}} = \frac{d_{\mathrm{SVT}}\rho_{\mathrm{PtBMA}}M_{\mathrm{PMAA}}}{\rho_{\mathrm{PMAA}}M_{\mathrm{PtBMA}}}\frac{1}{U} \qquad (1)$$

where $d_{\mathrm{SVA}}^{\mathrm{dry}}$ is the calculated film thickness of a dry film after hydrolysis, d_{SVT} the film thickness of an unhydrolyzed film, and U the degree of hydrolysis. The densities of PtBMA and PMAA amount to $\rho_{\mathrm{PtBMA}} = 1.022$ g/cm^3 and $\rho_{\mathrm{PMAA}} = 1.170$ g/cm^3, respectively. The molecular weights of these polymers are $M_{\mathrm{PtBMA}} = 142$ kg/mol and $M_{\mathrm{PMAA}} = 86$ kg/mol, respectively. Assuming complete hydrolysis, $U = 1$, the dry film thickness should amount to $d_{\mathrm{SVA}}^{\mathrm{dry}} = 20 \pm 3$ nm. From a comparison with the experimental result of $d_{\mathrm{SVA}} = 26 \pm 3$ nm after hydrolysis, we can estimate the degree of swelling to $d_{\mathrm{SVA}}/d_{\mathrm{SVA}}^{\mathrm{dry}} = 1-1.3$ for films measured at ambient conditions.

We note that, after hydrolysis and drying, we observe a somewhat broader distribution of protrusion heights (Figure 2b) as compared to that of the virgin structure (Figure 2a). This effect most likely results from the drying process, as no such effect is observed when the films are imaged in water. AFM experiments in water have been performed to study the response of the structure to changes in pH. In water, the films swell further and the degree of swelling is found to depend on pH (see below). Before we turn to a detailed analysis of this pH dependence we note that imaging in water is considerably more demanding experimentally as the structures become extremely soft. As an example, in Figure 2e,f we show typical SFM height images taken in water at pH 6. Both parts of the figure show a hexagonal arrangement of protrusions. While Figure 2e exhibits a granular structure with the highest thickness being in the middle of the protrusions, Figure 2f shows indentations on top of the protrusions. We assume that the differences may be due to different amounts of indentation of the SFM tip into the swollen polymer structure and consequently may not reflect real differences in the physical structure of the film. Since we are not able to relate the difference between parts e and f of Figure 2 to any controlled change of experimental conditions, we will not further discuss their origin. For the following discussion, it will suffice to identify the structure as a hexagonal arrangement of protrusions irrespective of the detailed structure of their top.

pH Dependence of the Microstructure. We turn to the influence of the pH value of the aqueous solution on the morphology and the film thickness of the hydrolyzed films.

In Figure 3 SFM height images taken in water at different pH values are displayed. Between pH 6 and pH 9 the same sample region has been measured; for convenience we have marked a "seven-ring" as a typical defect of the hexagonal pattern by a white box. At low pH (pH $\leq$ 6) the surface morphology remains the same as shown in Figure 2e,f above: the surface is characterized by a hexagonal array of protrusions with a characteristic height of 20 nm. At higher pH values, however, the pattern changes significantly. What appear as protrusions at pH $\leq$ 6 turn into holes at pH $>$ 6. Imaging the same position of the surface at different pH values enables us to confirm that the holes indeed appear at the positions of the protrusions. As a consequence, the overall hexagonal arrangement of the pattern does not change. The characteristic in-plane length of the hexagonal structure remains unchanged as well (protrusion-to-protrusion and hole-to-hole distance $L = 80 \pm 5$ nm). Therefore, we are led to conclude that the PS skeleton of the perforated lamella does not change during the pH variation.

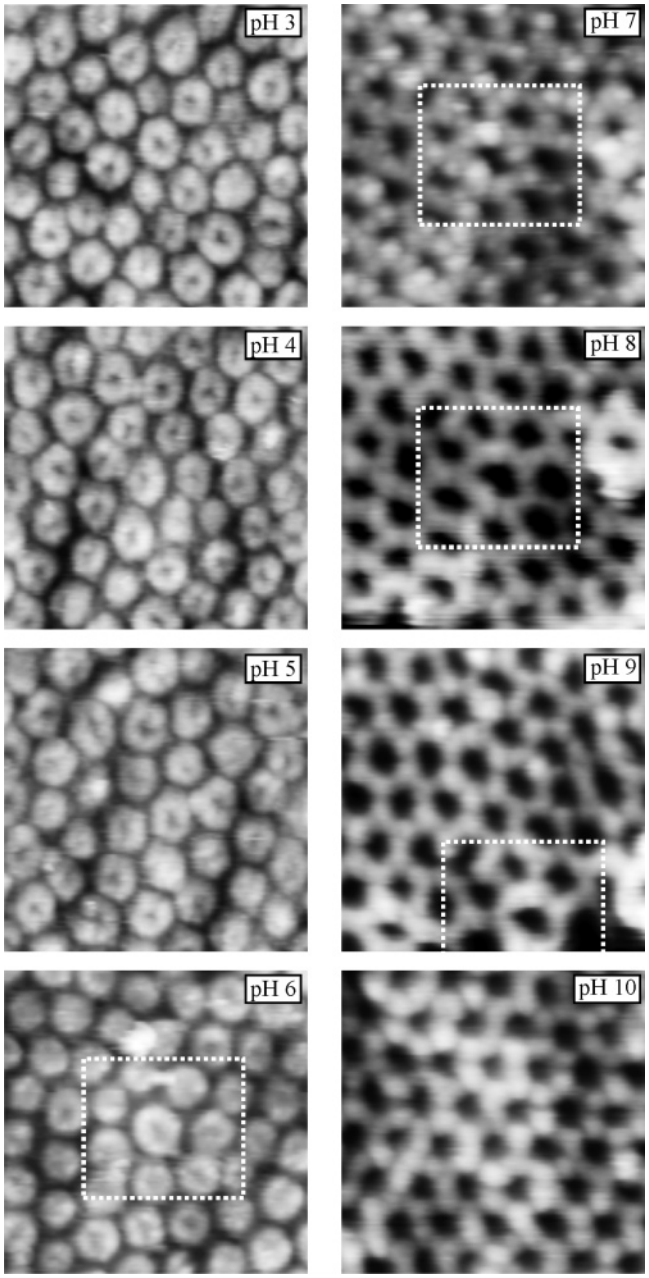

Figure 3. SFM height images of a single layer of PL at different pH values of the buffer solution. The image size is 500×500 nm^2. The height scale for pH 3−6 is $\Delta z = 0-30$ nm, and $\Delta z = 0-80$ nm for pH 7−10. The white box marks the same sample position.

Before we turn to a discussion of the above findings, it is interesting to quantitatively follow the overall film thickness as a function of pH. In Figure 4, we display the film thickness in the swollen state normalized to the dry film thickness as a function of pH. The data points correspond to different samples, and the degree of swelling has always been calculated relative to the thickness observed for the particular sample after hydrolysis in the dry state. Below pH 6 the film thickness stays constant, while between pH 6 and pH 8 we find a sharp increase in the degree of swelling. At

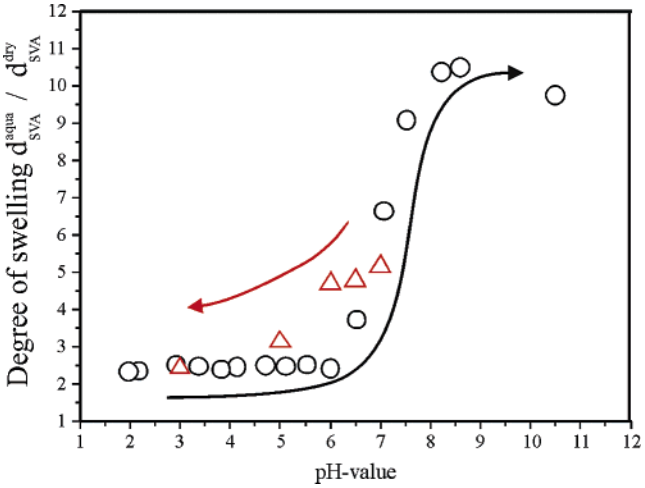

Figure 4. Degree of swelling as a function of pH. After the maximum pH value was reached (curve of black circles), the pH was decreased to the starting point (red triangles).

pH > 8 the degree of swelling levels off at a value of $d^{aqua}_{SVA}/d^{dry}_{SVA} \approx 10.5$. For pH ≥ 10 we were not able to get reliable data because of imaging problems. We note that the swelling of the films is reversible. The red triangles displayed in Figure 4 indicate the degree of swelling when the pH value is decreased. At low pH the film thickness reaches a minimum value which is in reasonable agreement with the original film thickness.

The third block of the triblock terpolymer, poly(methacrylic acid), is known to undergo a transition from a contracted to an expanded state around pH = pK_a = 5 in solution. The conformational change is induced by the repulsion between the increasing number of carboxylate anion groups. The chains resist expansion before a critical charge density is attained. This fact has been interpreted as being due to a hypercoiled conformation of PMAA in the un-ionized state which is stabilized through hydrophobic interactions between the methyl substituents of PMAA and hydrogen-bonding forces.[41−44] The sharp increase of the film thickness and the changes of the lateral structures from protrusions to holes appear at pH > 6 for our system, which is well above the pK_a of PMAA. Apparently the thin film results on block copolymers containing PMAA do not fully reflect the solution behavior of the PMAA homopolymer. At pH less than 6 the PMAA seems not to respond to any changes of the surrounding medium. Probably methyl−methyl and hydrogen-bonding forces have a stabilizing effect on the PMAA chains, but additionally the particular microdomain structure may play an important role. We have chemically modified a frozen surface structure which is confined to a certain film thickness. Only at a certain degree of ionization, higher than the pK_a, can the PMAA chains undergo a rearrangement from the contracted form, which is given by the dimensions of the PL phase, to an extended form. While at low charge densities the chain entropy and the confinement of the material tend to keep the polymer configuration as close to Gaussian statistics as possible, at a certain charge density stretching of the coils is favored. Probably similar to the homopolymer in solution, first free COOH groups are ionized, which are mainly located at external regions of the coil and/or at the top surfaces of the film. The deprotonation of the inner groups can be regarded as the beginning of the transformation.[42] Up to pH 6, water is hindered from entering the film (constant film thickness), and at pH > 6, the water uptake and the mobility of the polymer chains increase, which is indicated by the strong increase of the film thickness (by orders of magnitude).

It is interesting to note that poly(2-vinylpyridine) should respond to the pH at low pH values (pH < 5).[45,46] The homopolymer is hydrophobic and insoluble in water at pH > 5, but ionized and water-soluble in acidic aqueous solutions at pH < 5. As neither the film thickness nor the morphology undergoes a transition at low pH values (pH < 6), we may assume that the presence of the PMAA matrix phase hinders significant structural changes of P2VP in the present investigations. Furthermore, the volume fraction of P2VP amounts only to $\phi_P = 20\%$ and may not be sensitive enough to detect the respective deswelling/swelling effects.

We now return to the changes in the surface structure displayed in Figure 3. If we combine the findings that (a) the overall lateral structure remains unchanged due to the stability of the PS perforated lamella core and that (b) the film thickness increases significantly due to chain stretching of PMAA above pH 6, we can come up with a model explaining the observed surface structures. At moderate degrees of swelling (pH ≤ 6, Figure 5a) the regions containing more of the hydrophilic PMAA block (i.e., the perforations of the PL structure) will swell more than the other areas, resulting in isolated protrusions appearing above the perforations of the PL phase. At high degrees of swelling (pH > 6, Figure 5b) the PMAA chains are significantly stretched. Since each PMAA chain is bound to the PS skeleton, at high chain stretching the surface structure will reflect the structure of the skeleton, leading to depressions located on top of the perforations of the PL phase. Here

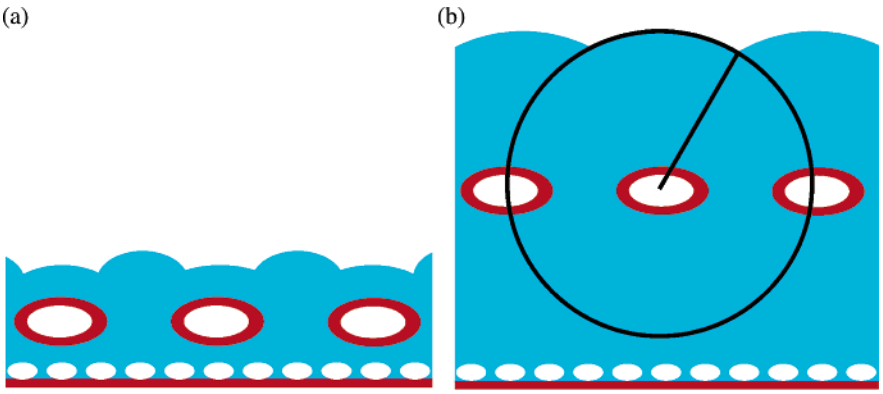

Figure 5. Sketches of the PL phase at pH < 6 (a) and pH > 6 (b).

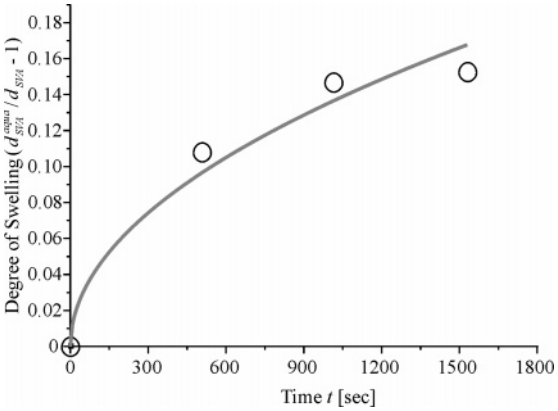

Figure 6. Degree of swelling at different times t at pH 7. The solid line represents a least-squares fit to the data using eq 3.

we assume that the chains can only stretch to a certain radius, which is indicated by the radius of the circle in the sketch of Figure 5b.

Figure 6 shows the degree of swelling as a function of the time at pH 7. We assume a Fickian diffusion behavior, which shows the following dependence for short times:

$$\frac{M_t}{M_\infty} = \left(\frac{16D}{l^2\pi}\right)^{1/2} t^{1/2} \tag{2}$$

Here, M_t and M_∞ are the masses of water within the polymer film at time t and in equilibrium, respectively. D is the diffusion coefficient, and $l = (d_{SVA} + d_\infty)/2$ is the thickness of the film, with d_{SVA} being the original film thickness ($t = 0$) and $d_\infty = 130$ nm the film thickness which can be determined with graphical extrapolation. Since

$$\frac{d_{SVA}^{aqua}}{d_{SVA}} - 1 = \frac{M_t}{M_\infty}\left(\frac{d_\infty}{d_{SVA}} - 1\right) \tag{3}$$

with d_{SVA}^{aqua} being the measured film thickness at times t, we have plotted $(d_{SVA}^{aqua}/d_{SVA} - 1)$ as a function of t in Figure 6. The continuous line indicates the fit of the data by eq 3. Though we have used a rather rough model to describe the diffusion behavior of water in thin films, the Fickian curve fits the data quite well. The diffusion coefficient can be determined to be $D = 1.7(\pm 1) \times 10^{-14}$ cm^2/s. For a more accurate evaluation it has to be taken into consideration that both the diffusion coefficient and the film thickness in thin films are not independent of the concentration, which is anticipated by the equations used above.

pH Dependence of Cylinder Structures. Finally, we note that the stability of the PL phase after hydrolysis is intimately connected with the continuous nature of the PS skeleton. In some of our specimens, the PL phase appears to coexist with a single layer of core−shell cylinders, i.e., with the bulk phase of the block terpolymer. Figure 7a shows an SFM image covering the transition between a perforated lamella structure and core−shell cylinders oriented parallel to the sub-

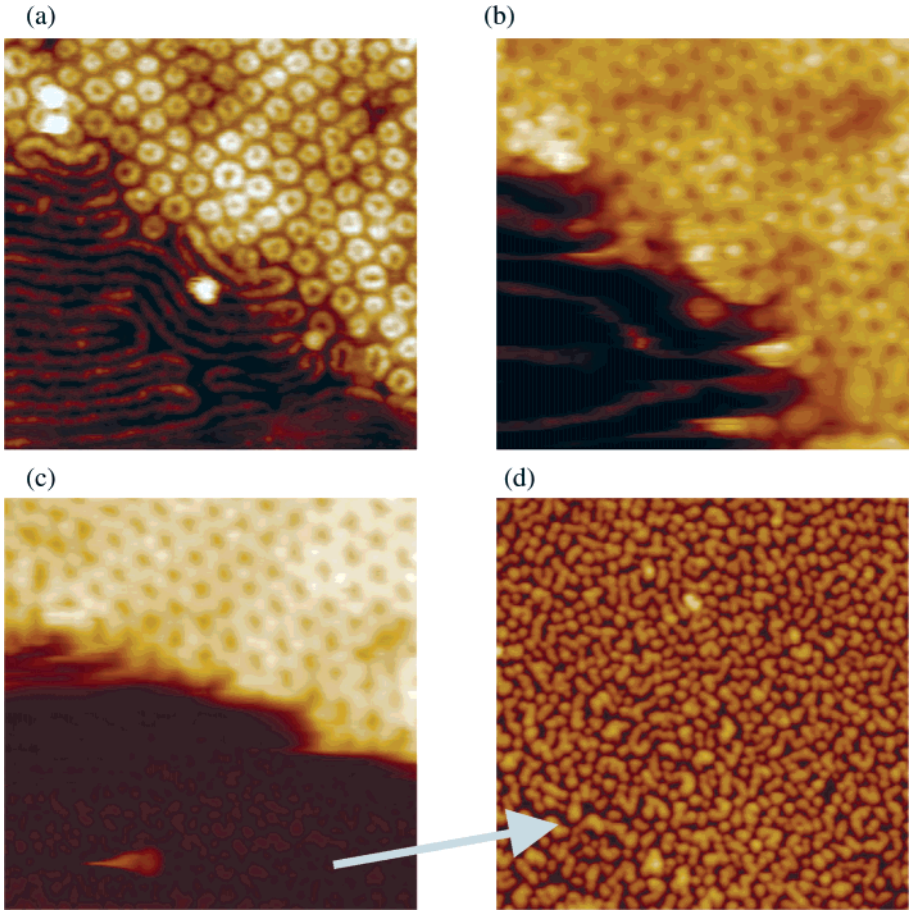

Figure 7. SFM height images (aqueous environment) of a transition between PL and cylinders oriented parallel to the surfaces ($C_{||}$) at pH 6 (a), pH 6.5 (b), and pH 7 (c). The image size is 1×1 μm^2. The height scales are $\Delta z = 0-30$ nm (a), $\Delta z = 0-160$ nm (b), and $\Delta z = 0-500$ nm (c). (d) shows the structure of an adsorbed polymer layer next to the substrate after removal of $C_{||}$.

strate after hydrolysis at pH ≤ 6. Similar to the above-described PL phase, the hydrolysis has apparently not altered the microdomain structure. To test the stability of both phases against changes in pH, parts b and c of Figure 7 show the same spot of the sample imaged at pH 6.5 and at pH 7, respectively. While the PL phase remains stable and undergoes the structural changes described in the previous section, the cylinders become unstable and eventually disappear. In contrast to the perforated lamella structure, where PS and P2VP act as a continuous skeleton for the overall structure, the core−shell cylinders are single objects embedded in a matrix of the strongly swollen PMAA. Due to the strong swelling of PMAA around pH 7 the entire cylinders may be dissolved.

Underneath the cylinders a thin disordered polymer layer remains (Figure 7d). This layer can be attributed to a wetting layer which is attached to the silicon substrate via the polar poly(2-vinylpyridine) block. These observations are in agreement with our former findings about the wetting layer next to the substrate in thin films of the unhydrolyzed triblock terpolymer.[34−36] We have found that irrespective of the chemical nature of the substrate a physisorbed, PtBMA-rich layer of about 10 nm thickness is found underneath the entire polymer film.

Conclusion

In conclusion, we have shown that a rather complex core−shell perforated lamella structure formed in a thin film of an ABC triblock terpolymer can be turned into a pH-responsive nanostructure via acid-catalyzed hydrolysis in a polymer-analogous reaction. The hydrolysis is found not to alter the perforated lamella structure, since the PS core of the structure is not affected by the treatment. While the lateral dimensions of the microstructure do not change within the experimental resolution (i.e., to within 5%), the thickness of the films increased to as much as 10 times the dry value. Therefore, the material seems to expand in a single dimension only. This feature may be of importance, when pH-responsive soft materials are used as switches or actuators in nanodevices. We note that irrespective of this finding we expect the PMAA chains to explore the full three-dimensional space on expansion. This is in line with the observed degree of swelling (Figure 4), which fits well to earlier results on similar systems.[41−44] It shall be an interesting extension of our work to create laterally patterned patches of the material and quantify the aspect ratio of the swelling process. A comparison between the perforated lamella phase and the cylinder phase indicates that the continuous nature of the PS skeleton appears essential for the mechanical stability of the overall structure during swelling.

Acknowledgment. We thank M. Lysetska for the help with the MultiMode scanning force microscope and R. Magerle and A. H. E. Müller for fruitful scientific discussions. We acknowledge financial support from the Deutsche Forschungsgemeinschaft (SFB 481).

References and Notes

(1) Bates, F. S.; Frederickson, G. H. *Phys. Today* **1999**, *52*, 32.
(2) Krausch, G. *Mater. Sci. Eng. Rep.* **1995**, *14*, 1.
(3) Fasolka, M. J.; Mayes, A. M. *Annu. Rev. Mater. Res.* **2001**, *31*, 323.
(4) Anastasiadis, S. H.; Russell, T. P.; Satija, S. K.; Majkrzak, C. F. *Phys. Rev. Lett.* **1989**, *62*, 1852.
(5) Walton, D. G.; Kellogg, G. J.; Mayes, A. M.; Lambooy, P.; Russell, T. P. *Macromolecules* **1994**, *27*, 6225.
(6) Matsen, M. W. *Curr. Opin. Colloid Interface Sci.* **1998**, *3*, 40.
(7) Kellogg, G. J.; Walton, D. J.; Mayes, A. M.; Lambooy, P.; Russell, T. P.; Gallagher, P. D.; Satija, S. K. *Phys. Rev. Lett.* **1996**, *76*, 2503.
(8) Binder, K. *Adv. Polym. Sci.* **1999**, *138*, 1.
(9) Krausch, G.; Magerle, R. *Adv. Mater.* **2002**, *14*, 1579.
(10) Mansky, P.; Chaikin, P.; Thomas, E. L. *J. Mater. Sci.* **1995**, *30*, 1987.
(11) Park, M.; Harrison, C.; Chaikin, P. M.; Register, R. A.; Adamson, D. H. *Science* **1997**, *276*, 1401.
(12) Cheng, J. Y.; Ross, C. A.; Chan, V. Z.-H.; Thomas, E. L.; Lammertink, G. H.; Vansco, G. J. *Adv. Mater.* **2001**, *13*, 1174.
(13) Thurn-Albrecht, T.; Schotter, J.; Kastle, G. A.; Emley, N.; Shibauchi, T.; Krusin-Elbaum, L.; Guarini, K.; Black, C. T.; Tuominen, M. T.; Russell, T. P. *Science* **2000**, *290*, 2126.
(14) Jeoung, E.; Galow, T. H.; Schotter, J.; Bal, A.; Ursache, M.; Tuominen, M.; Stafford, C. M.; Russell, T. P.; Rotello, V. M. *Langmuir* **2001**, *17*, 6396.
(15) Kim, H.-C.; Jia, X.; Stafford, C. M.; Kim, D. H.; McCarthy, T. J.; Tuominen, M.; Hawker, C. J.; Russel, T. P. *Adv. Mater.* **2001**, *13*, 795.
(16) Advincula, C. A., Brittain, W. J., Cast, K. C., Rühe, J., Eds. *Polymer Brushes*; Wiley-VCH: Weinheim, Germany, 2004.
(17) Biesalski, M.; Johannsmann, D.; Rühe, J. *J. Chem. Phys.* **2002**, *117*, 4988.
(18) Guo, X.; Weiss, A.; Ballauff, M. *Macromolecules* **1999**, *32*, 6043.
(19) Guo, X.; Ballauff, M. *Phys. Rev. E* **2001**, *64*, 051406.
(20) Dautzenberg, H.; Jaeger, W.; Kötz, J.; Philipp, B.; Seidel, C.; Stscherbina, D. *Polyelectrolytes*; Hanser: Munich, 1994; p 272.
(21) Kamachi, M.; Kurihara, M.; Stille, J. K. *Macromolecules* **1972**, *5*, 161.
(22) Ramireddy, C.; Tuzar, Z.; Prochazka, K.; Webber, S. E.; Munk, P. *Macromolecules* **1992**, *25*, 2541.
(23) Patrickios, C. S.; Hertler, W. R.; Abbottt, N. L.; Hatton, T. A. *Macromolecules* **1994**, *27*, 930.
(24) Bronstein, L. M.; Sidorov, S. N.; Valetsky, P. M. *Langmuir* **1999**, *15*, 6256.
(25) Gohy, J.-F.; Antoun, S.; Jérôme, R. *Macromolecules* **2001**, *34*, 7435.
(26) Qin, S.-H.; Qiu, K.-Y. *J. Polym. Sci., Part A: Polym. Chem.* **2001**, *39*, 1450.
(27) Bieringer, R.; Abetz, V.; Müller, A. H. E. *Eur. Phys. J. E* **2001**, *5*, 5.
(28) Giebeler, E.; Stadler, R. *Macromol. Chem. Phys.* **1997**, *198*, 3815.
(29) Förster, S.; Schmidt, M. *Adv. Polym. Sci.* **1995**, *120*, 53.
(30) Kassapidou, K.; Jesse, W.; Kuil, M. E.; Lapp, A.; Egelhaaf, S.; van der Maarel, J. R. C. *Macromolecules* **1997**, *30*, 2671.
(31) Hamley, I. W. *The Physics of Block Copolymers*; Oxford University Press: Oxford, 1998.
(32) Liu, G.; Ding, J.; Stewart, S. *Angew. Chem., Int. Ed.* **1999**, *38*, 835.
(33) Ludwigs, S.; Böker, A.; Abetz, V.; Müller, A. H. E.; Krausch, G. *Polymer* **2003**, *44*, 6815.
(34) Ludwigs, S.; Böker, A.; Voronov, A.; Rehse, N.; Magerle, R.; Krausch, G. *Nat. Mater.* **2003**, *2*, 744.
(35) Ludwigs, S.; Schmidt, K.; Stafford, C.; Fasolka, M.; Karim, A.; Amis, E.; Magerle, R.; Krausch, G. *Macromolecules* **2005**, *38*, 1850.
(36) Ludwigs, S.; Zvelindovsky, A. V.; Sevink, G. J. A.; Krausch, G.; Magerle, R. *Macromolecules* **2005**, *38*, 1859.
(37) Esker, A. R.; Mengel, C.; Wegner, G. *Science* **1998**, *280*, 892.
(38) Mengel, C.; Esker, A. R.; Meyer, W. H.; Wegner, G. *Langmuir* **2002**, *18*, 6365.
(39) Jeon, C. H.; Makhaeva, E. E.; Khokhlov, A. R. *Macromol. Chem. Phys.* **1998**, *199*, 2665.
(40) Elbs, H.; Fukunaga, K.; Sauer, G.; Stadler, R.; Magerle, R.; Krausch, G. *Macromolecules* **1999**, *32*, 1204.
(41) Arnold, R. *J. Colloid Sci.* **1957**, *12*, 549.
(42) Dong, K.; Tsubahara, N.; Fujimoto, Y.; Ozaki, Y.; Nakashima, K. *Appl. Spectrosc.* **2001**, *55*, 1603.
(43) Morawetz, H. *Macromolecules* **1996**, *29*, 2689.
(44) Nakashima, K.; Fujimoto, Y.; Anzai, T.; Dong, J.; Sato, H.; Ozaki, Y. *Bull. Chem. Soc. Jpn.* **1999**, *72*, 1233.
(45) Puterman, M.; Koenig, J. L.; Lando, J. B. *J. Macromol. Sci., Phys.* **1979**, *B16*, 89.
(46) Martin, T. J.; Prochazka, K.; Munk, P.; Webber, S. E. *Macromolecules* **1996**, *29*, 6071.

MA047812Q